AD-A055 419 AIR FORCE INST OF TECH WRIGHT-PATTERSON AFB OHIO SCH--ETC F/G 20/5
CHARACTERIZATION OF HIGH POWER GAAS LASERS.(U)
DEC 77 D J MURAWINSKI

UNCLASSIFIED AFIT/GEP/PH-77-9 NL

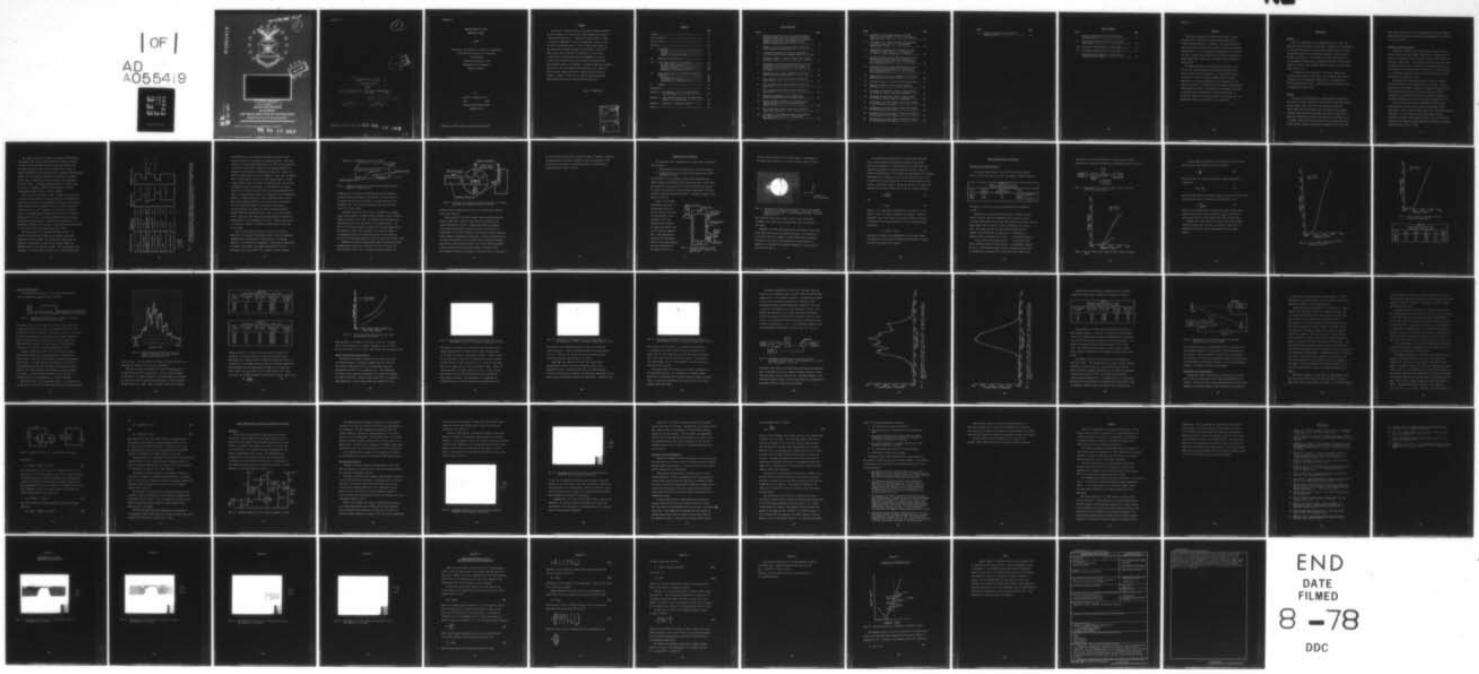

END
DATE FILMED
8 -78
DDC

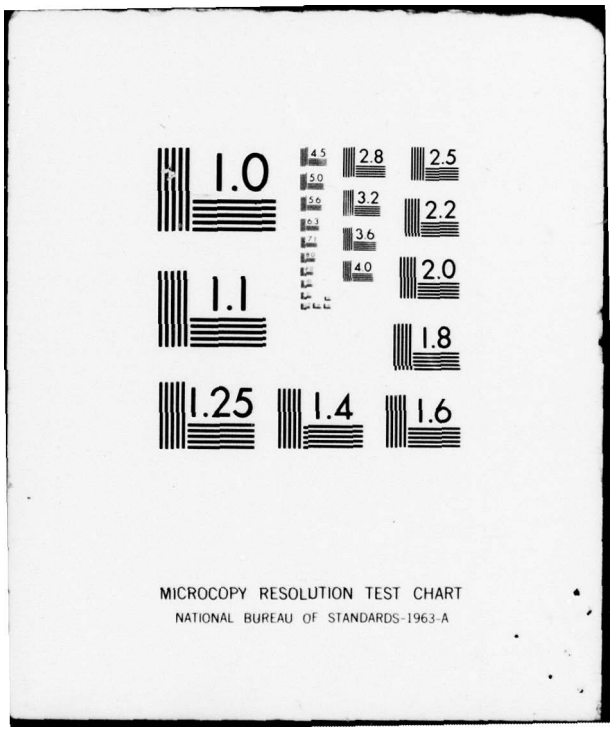
1.0
1.1
1.25
1.4
1.6
1.8
2.0
2.2
2.5
2.8
3.2
3.6
4.0
4.5
5.0
5.6
6.3
7.1
MICROCOPY RESOLUTION TEST CHART
NATIONAL BUREAU OF STANDARDS-1963-A

UNITED STATES AIR FORCE

AIR UNIVERSITY

AIR FORCE INSTITUTE OF TECHNOLOGY

Wright-Patterson Air Force Base, Ohio

GEP/PH/77-9

(1)

(6) CHARACTERIZATION OF HIGH POWER GaAs LASERS.

THESIS

(14) AFIT/GEP/PH/77-9 (10) Daniel J. Murawinski
Capt USAF

(9) Master's thesis,

(11) Dec 77 (12) 66p.

GEP/PH/77-9

CHARACTERIZATION OF HIGH POWER GaAs LASERS

THESIS

Presented to the Faculty of the School of Engineering

of the Air Force Institute of Technology

Air University

in Partial Fulfillment of the

Requirements for the Degree of

Master of Science

by

Daniel J. Murawinski, B. S.

Capt USAF

Graduate Engineering Physics

December 1977

Preface

It has been a long time since I have had the chance to write in the first person, so I hope you will enjoy reading this as much as I have enjoyed writing it. I chose this thesis because I thought it would be a challenge: I was not disappointed. However, I did not meet the challenge alone. I wish to thank George Gergal for the untold hours he spent working on the RF driver. Had it not been for him, there would not be a Chapter IV to this thesis. I would like to thank Dr Luke for the encouragement he gave me at the times I needed it most, and the help he provided during many different phases of my research. I thank the AFAL for proposing the thesis to AFIT and supplying the laboratory, and I thank Dr Knecht for the personal interest he showed toward me during my research. Finally, I would like to thank my wife and children whose patience with me was exceeded only by their love.

Daniel J. Murawinski

Contents

List of Figures

List of Tables

Abstract

High power, cryogenically operated, dual cavity, ternary heterostructure, GaAs lasers are characterized under CW and 25 MHz RF current modulation conditions. The CW characteristics that are measured include: power, spectral, spatial, and temporal characteristics. It is calculated that degradation of one cavity will cause complete laser failure when the laser is operated near maximum rated drive current due to the dual cavity structure of these devices.

RF current modulation at 25 MHz causes the lasers to fail within a few hours, although the same lasers exhibited stable operation under CW drive conditions. It is postulated that the piezoelectric effect in the GaAs material causes the rapid degradation, but further refinements in the calculation of the shear force present in the GaAs material is needed before definite conclusions can be made. The increase in the average output power of the GaAs lasers, operated with RF current modulation, is empirically related tc the AC input power of the signal, but the mechanism by which this can occur is not understood.

Introduction

General

Since its introduction as an operational device in 1962, the GaAs laser has been improved a great deal. Advances in the fabrication of these devices have led to commercially available GaAs lasers that consistently produce 100 mw CW output power (Ref 1: 1535); however, further optimization in the fabrication of GaAs lasers has led to the development of high power, cryogenically operated, CW GaAs lasers capable of optical output emission levels in excess of 2.0 w average power (Ref 2: 1-2).

In systems now using GaAs lasers, the present commercially available GaAs lasers are sufficient, but two military applications, illuminators and rangefinders, require the use of high power RF current-modulated GaAs lasers. Relatively little work has been done to characterize these lasers.

Problem

The goal of this research was to characterize the behavior of high power, RF current-modulated, liquid nitrogen cooled GaAs lasers, and to compare these results to the same lasers operated CW. Perkin-Elmer Corp has conducted brief experiments in this regard, and these experiments have shown that 100 per cent modulation of high power cryogenically operated GaAs lasers can be achieved at up to 25 MHz. This effort has also shown that the average power from the RF current-modulated GaAs lasers was larger than that from the

same lasers operated CW, but this program did not determine complete behavioral characteristics, optimum operating parameters or lifetime of the lasers (Ref 3).

Summary of Current Knowledge

Stimulated emission in GaAs diode lasers is unique in that optical transitions occur between distributions of energy states in valence and conduction bands rather than between discrete atomic or molecular energy levels. These optical transitions occur as a result of carrier recombination in a volume of the laser material near to and including the junction region. The size of this volume depends on the diffusion length of the injected minority carriers, and the structure of the GaAs diode laser.

Early GaAs lasers were homostructure devices that required very high threshold current densities (J_{th}) for lasing. The J_{th} required for these lasers to operate was high partly because of the thick recombination region due to minority carrier diffusion. In addition, the optical field was in an inefficient waveguide of uncertain dimensions, and the internal quantum efficiency was low.

Now, most GaAs diode lasers are designed as multi-layered heterostructure devices, and are grown by liquid phase epitaxy (LPE) (Ref 1: 1512). Such structures provide both carrier and optical confinement to a thin region: a region much thinner than the recombination region of homostructure lasers. Carrier and optical confinement has reduced J_{th} significantly and increased the internal quantum efficiency (Ref 1: 1512).

The lasers used in this research are ternary heterostructure (TH) devices built by Laser Diode Laboratories (under contract to the AFAL: contract # F33615-75-C-1100) using the method of LPE. This particular diode laser structure evolved from a study of various GaAs-GaAlAs multi-heterostructures to determine which structure offered the best cryogenic performance with respect to threshold current (I_{th}), differential quantum efficiency, beam divergence, and power output. A schematic representation of a TH diode laser as well as its bandgap, refractive index profile, and doping concentrations appear in Fig. 1 (Ref 2: 1,10,23).

The x, y, and z subscripts in Fig. 1 indicate the proportions of Ga and Al atoms present in each epitaxial layer. Qualitatively, the numerical values of these subscripts are related to the bandgap energy (E_g) and index of refraction (n) in the following manner: as the value of x, y, or z increases in the respective epitaxial layers, the bandgap energy increases while the index of refraction decreases (Ref 1: 1512). This was determined from photoresponse measurements of $(Ga_{1-x}Al_x)As$. By relating the photocurrent to the absorption cofficient of the material for different melt compositions, one can then determine the change in E_g (Ref 4: 4911).

The first layer of the epitaxial structure in Fig. 1 is n-type GaAs material which serves as the substrate upon which successive layers are grown. The second layer, n-type GaAs, is grown onto the substrate to serve as an interface between the (GaAl)As layer and the substrate material. The second layer is not necessary to the active laser structure, but it covers microscopic

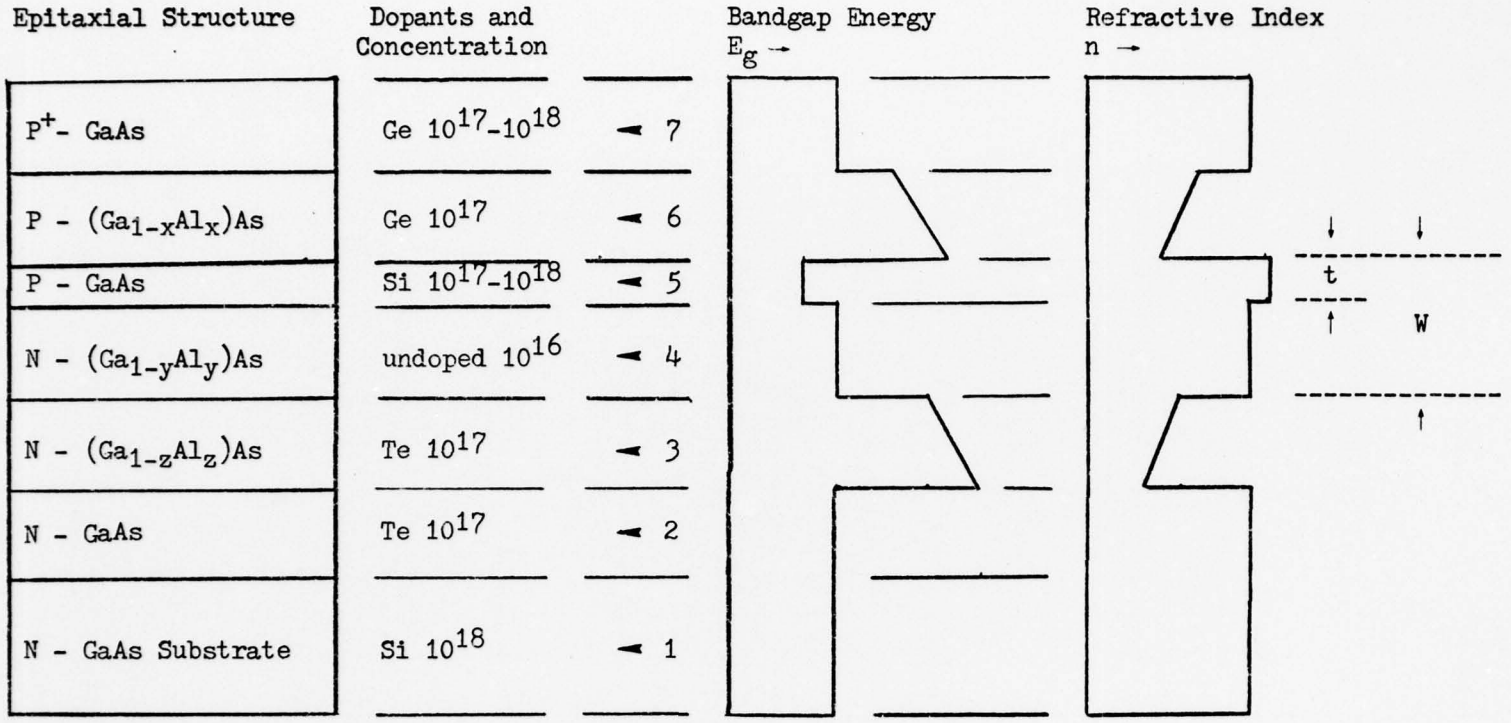

$x = 0.40$
$y = 0.03$
$z = 0.10$

Fig. 1. Schematic representation of GaAs-(GaAl)As ternary heterostructure diode laser showing its epitaxial structure, dopants and concentration (cm^{-3}) (Ref 5), bandgap energy profile, and refractive index profile (adapted from Ref 2: 10).

non-uniformities of the substrate material and provides a flat uniform interface for the growth of subsequent layers. Layer three consists of n-type (GaAl)As doped with Te to 10^{17} (cm^{-3}), and serves to confine the stimulated emission to the optical waveguide, W, through its heterojunction interface with layer four. Layers four and five together form the optical waveguide. Layer four, the passive part of the waveguide, consists of either lightly doped or undoped n-type (GaAl)As, forms the bulk of the optical cavity, and contains the depletion region of the diode. The remainder of the cavity, layer five, is p-type GaAs which serves as the active/recombination region. As was mentioned earlier, the thickness of the recombination region, t, strongly affects the laser's threshold current density and internal quantum efficiency. Layer six limits the thickness of the recombination region to 0.9 μm (Ref 2: 23) because its heterojunction with layer five forms a potential barrier to confine electrons, injected from layer four, to the active layer (five). Layer six also serves as an optical barrier to confine the laser radiation to the waveguide region (W). Finally, layer seven, a p^+ GaAs cap, is grown to facilitate ohmic contact to the p side of the laser.

After the TH structure is grown, it is cut into pellets. Each pellet is a separate laser module which is then cut lengthwise, perpendicular to and through the active layer, in a direction parallel to the direction of propagation. A dual cavity laser module is formed in this manner, and appears schematically in Fig. 2. The purpose of the dual cavity is to reduce the laser's thermal

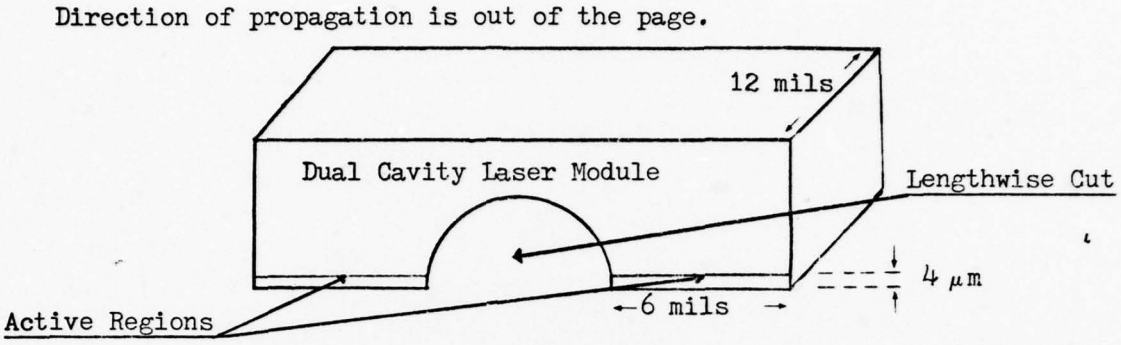

Fig. 2. Drawing of a dual cavity laser module showing its active regions and lengthwise cut.

impedance, and to increase its differential quantum efficiency. A high reflectivity coating is then applied to the rear facet of the laser, and the laser is mounted on a single-sided heat sink designed to fit into a Cryogenic Associates model IR-14R dewar (Ref 2: 10, 12-13, 27-31).

The laser heat sink, shown in Fig. 3, consists of a primary copper mounting block, a beveled pedestal submount, and an insulated negative electrode (Ref 2: 28). The primary copper mounting block bolts directly onto the cold finger of the cryogenic dewar. The bevel on the submount permits the diode to be set far enough back on the submount to permit heat generated in the junction region to be dissipated evenly in all directions, while it also reflects a portion of the beam back toward the center of each junction (Ref 2: 30).

Modulation of double-heterostructure (DH) diode lasers has been accomplished at rates up to 1 GHz with a DC bias of 10 per cent above threshold (Ref 6: 34). Although the laser structure of a

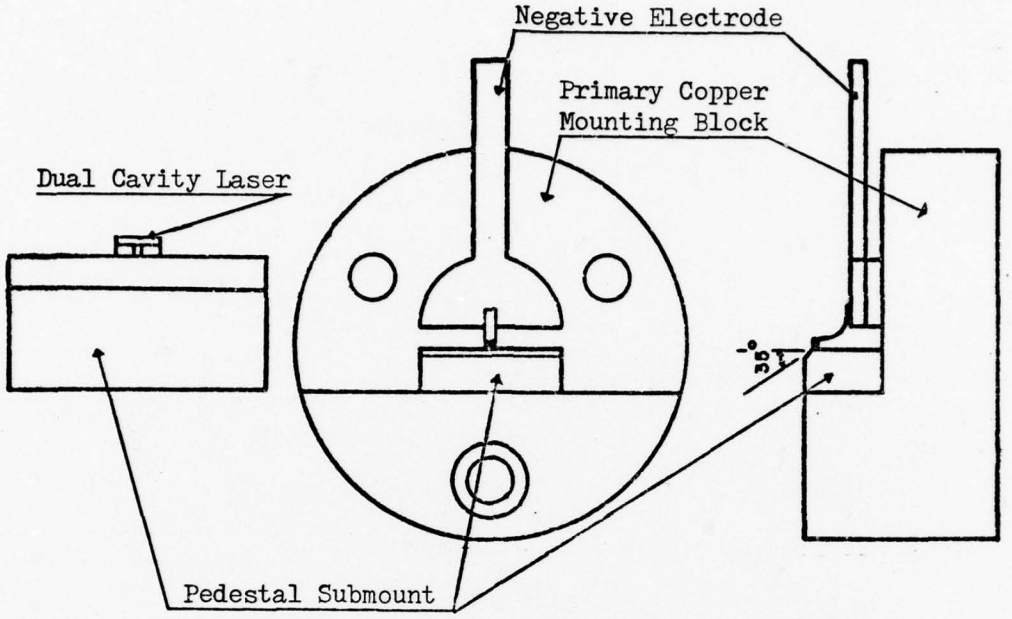

Fig. 3. A drawing illustrating the various components of the diode laser heat sink (adapted from Ref 2: 29, 32).

DH diode laser is different from that of a TH diode laser, similar results are expected.

Chown et al (Ref 6: 34-36) obtained clearly resolved modulated optical output from a DH diode laser that was DC biased and RF current-modulated at one GHz. A phase delay between the optical output and modulated current input was noted, but this was to be expected due to the finite lifetime of the injected minority carriers before radiative recombination takes place. It was determined that if the laser was modulated in such a manner that the current alternated from above to below threshold current, the output modulation pattern became oscillatory and less clearly defined. The cause is the time required for electron densities in the active layer to build up to

the level needed for gain after threshold current is reached. Therefore, by operating the laser with a modulation depth (see Appendix C) that is above I_{th}, the output of the laser will have a clearly defined modulation pattern (Ref 6: 34-36).

Experimental Preliminaries

The experiment used to characterize the GaAs lasers was divided into two parts:

1. Characterization of the lasers while they were DC driven.
2. Characterization of the lasers while they were RF current-modulated at 25 MHz.

For both parts of the experiment, Laser Diode Laboratories THR series ternary heterostructure diode lasers were used. These lasers were grown from the same melt by the LPE method discussed earlier. The lasers were operated at liquid nitrogen temperature (77°K) in a Cryogenic Associates model IR-14R dewar. A schematic diagram of the dewar is in Fig. 4.

Early in the CW characterization experiment, it was determined that the optical window of the dewar was aperturing the beam; therefore, the 2.5 cm diameter quartz window of the dewar was replaced with a 2.8 cm diameter sapphire flat. This modification eliminated the aperturing effect of the dewar geometry. The laser was mounted in the dewar 1.54 ± 0.1 cm

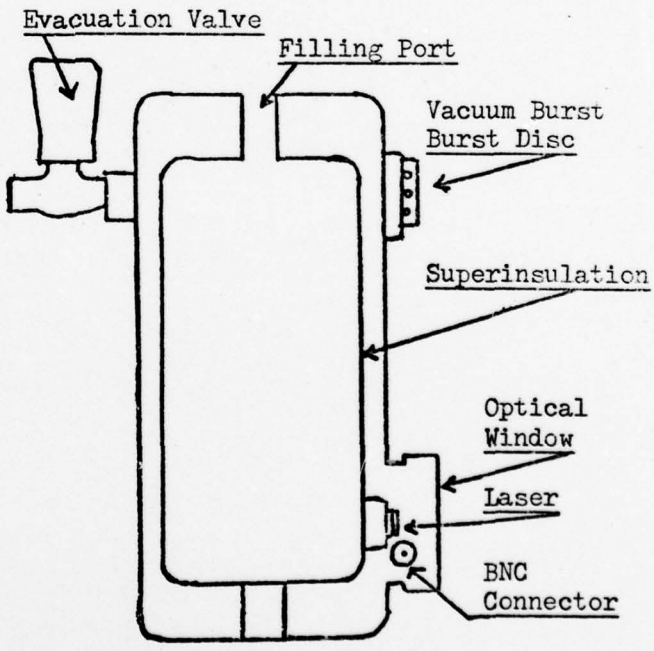

Fig. 4. Schematic diagram of liquid nitrogen dewar (adapted from Ref 2: 37).

from the outside surface of the optical window. A photograph of the diode laser oriented as it is in the dewar is shown in Fig. 5.

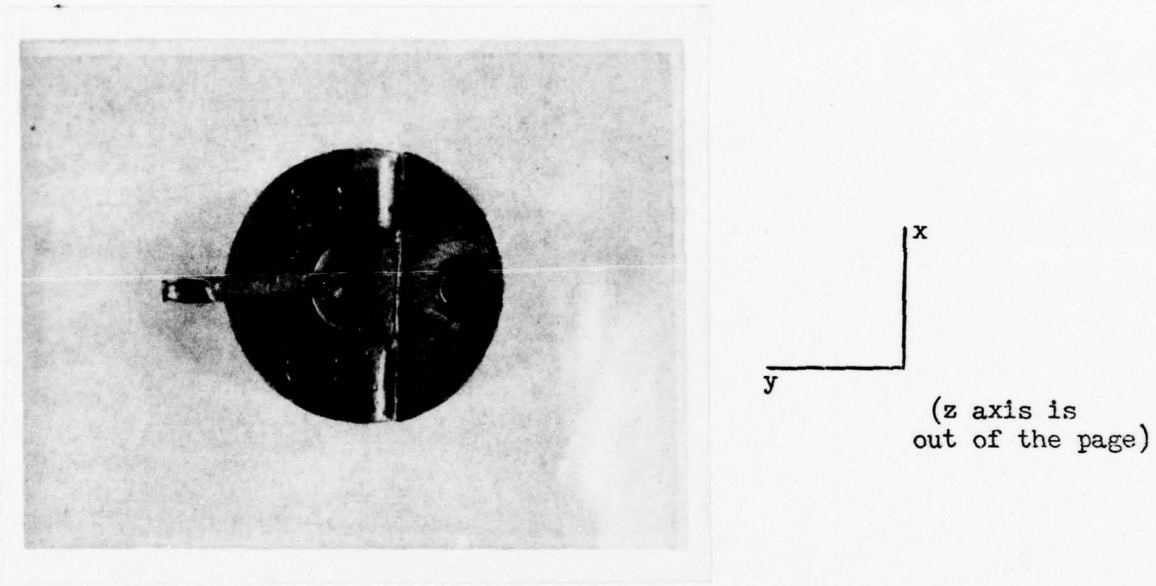

Fig. 5. Photograph of a diode laser oriented as if one were looking into the optical window of the dewar. A reference coordinate system is to the right of the photograph (see Fig. 3 for laser module position).

The coordinate axes chosen in Fig. 5 will be used consistently throughout this report when specifying directions with respect to the lasers.

Appendix A contains photographs of the front facet of each dual cavity laser used during this experiment prior to its installation in the dewar (with the exception of laser THR 6 which was already installed in the dewar). The orientation of the photographs in Appendix A is the same as the schematic drawing of the dual cavity laser shown in Fig. 2.

All radiometric measurements of the laser output were made with a Coherent Radiation Laboratories model 201 power meter. For these measurements, the detector head of the power meter was placed flush against the optical window of the dewar. Since the largest beam divergence of these lasers was approximately 10-12 degrees half-angle and the diameter of the detector head was 2.6 cm, it is estimated that at least 95 per cent of the beam was incident on the detector. Reflection losses at the optical window of the dewar were computed from Fresnel's formula (Ref 7: 42) for normal incidence,

$$R = \left(\frac{n-1}{n+1}\right)^2 \tag{1}$$

with

$$n = n_2/n_1 \tag{2}$$

where $n_1 = 1.0$, the index of refraction for air, and $n_2 = 1.76$ (Ref 8: 6-40), the index of refraction for sapphire. Since the reflection loss on both sides of the optical window is the same, the fraction of the beam transmitted through the optical window is given by

$$T = (1-R)^2 = 0.854 \tag{3}$$

Therefore, all output power measurements in this report should be increased by 14.6 per cent (unless stated otherwise) to obtain the true output power of the lasers.

Laser Characterization (DC Driven)

DC Output Power Characteristics

The lasers characterized in the DC driven mode are listed in Table I in the order they were used. The number of thermal cycles is

TABLE I
Hours of operation and status of each laser DC characterized

Laser	Hrs of Operation	Number of Thermal Cycles	Status
THR 6	13.8	10	partial degradation
THR 7	5.5	4	failure
THR 4	10.8	4	used in RF experiment

the number of times the lasers were cooled from room temperature to 77°K.

Measurements of the laser output power as a function of drive current were made using the experimental set-up shown in Fig. 6. The lasers were powered with a Trygon model HR40-5 power supply, but any power supply with an output of 3.5 A at approximately 10 V can be used. The current through the diode laser was monitored on a Triplett model 630 VOM, and the laser bias was monitored on a Tektronix 7514 oscilloscope with a 7D-13 digital multimeter plug-in.

A plot of the output power versus DC drive current for laser THR 6, obtained during the initial phase of the experiment, appears in Fig. 7. The threshold current (I_{th}) is determined from the plot by extending the linear portion of the curve to the current axis;

the current value that corresponds to the point where the curve deviates from linearity is defined as the threshold current (see Fig. 7).

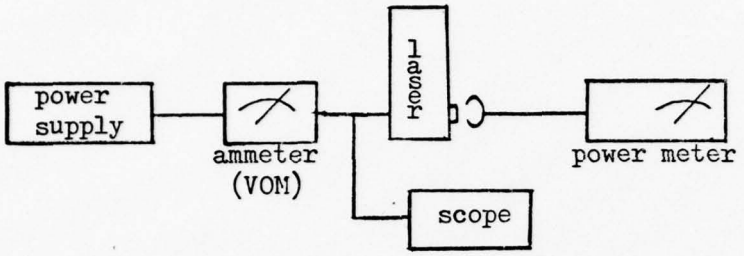

Fig. 6. Experimental set-up used to measure output power from the DC driven diode lasers.

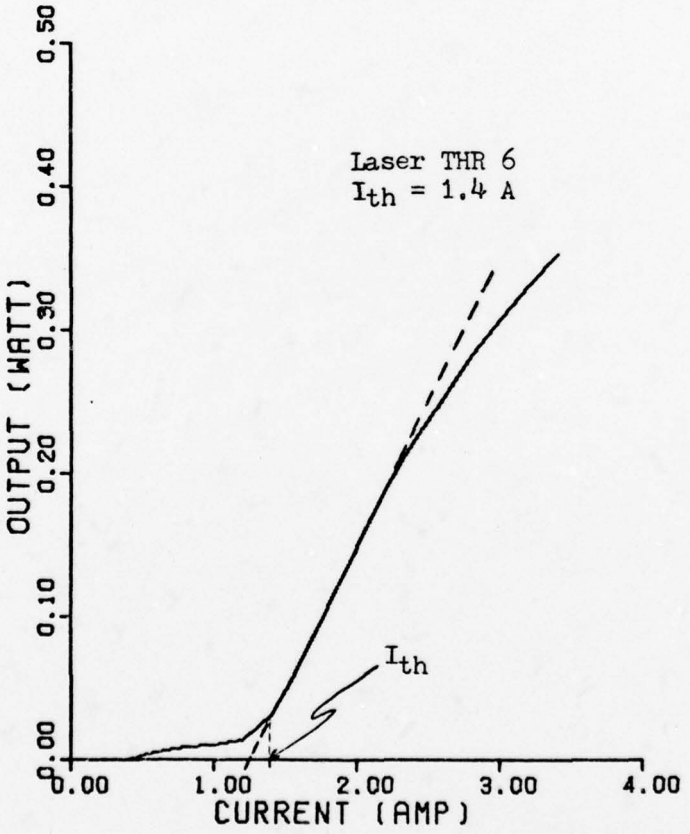

Fig. 7. Plot of output power versus DC drive current for laser THR 6.

A linear regression performed on the data points in the linear portion of the curve gives the slope of the curve.

$$m = \frac{\Delta P}{\Delta I} \tag{4}$$

From this value, the external differential quantum efficiency is computed as,

$$\eta_{ext} = \frac{m}{E_g} \tag{5}$$

where the value used for the energy bandgap, E_g, is 1.45 V (Ref 2: 39). The power efficiency of the lasers is given by (Ref 2: 35),

$$\gamma = \frac{P_o}{I_{max} V_f} \tag{6}$$

where P_o is the output power at maximum rated drive current which includes the power lost due to reflection, I_{max} is the maximum rated current, and V_f is the forward bias of the diode at I_{max}.

Figures 8 and 9 are plots of the output power versus DC drive current for lasers THR 7 and THR 4 respectively, while Table II summarizes the DC power output characteristics of the lasers tested.

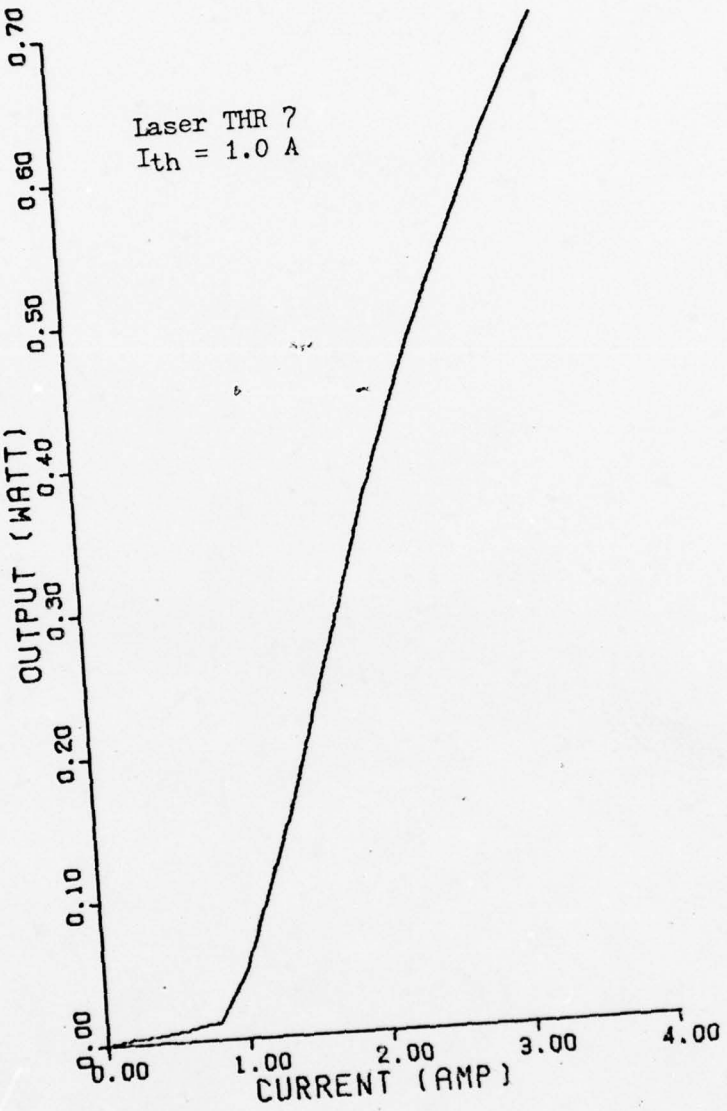

Fig. 8. Plot of output power versus DC drive current for laser THR 7.

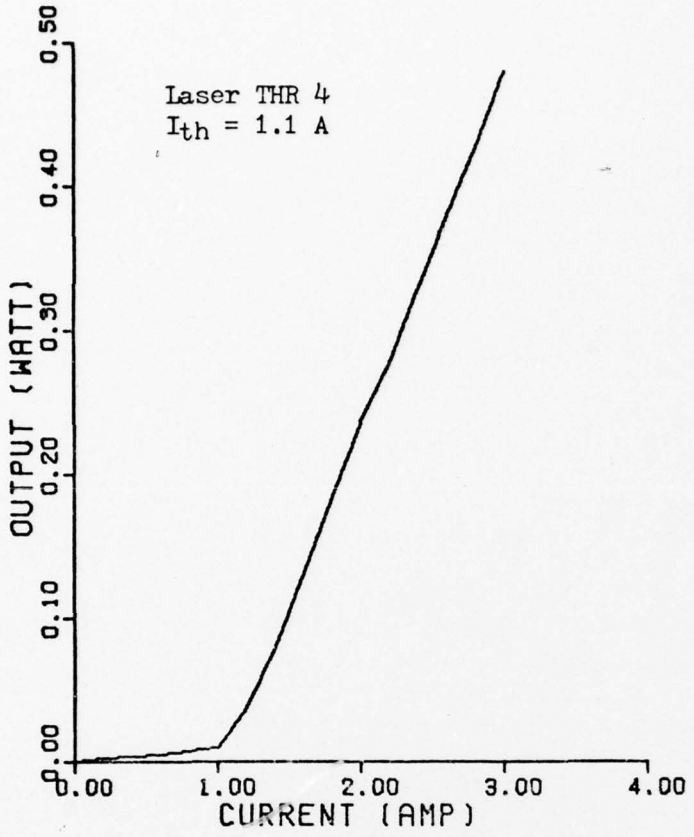

Fig. 9. Plot of output power versus DC drive current for laser THR 4.

TABLE II
Output power characteristics of the DC driven diode lasers

Laser	I_{th} (amps)	I_{max} (amps)	P_o (watts)	γ (%)	η_{ext} (%)
THR 6	1.4	3.5	0.41	2.9	13.3
THR 7	1.0	3.5	0.83	5.0	21.4
THR 4	1.1	3.0	0.49	4.2	17.0

Spectral Characteristics

The spectral characteristics of the lasers were determined from the experimental apparatus shown in Fig. 10.

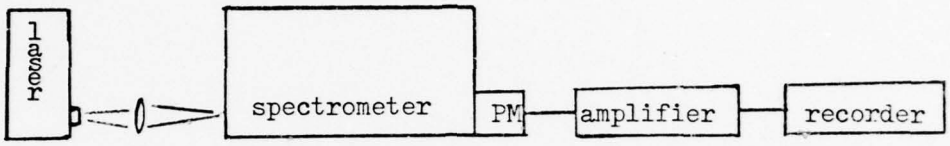

Fig. 10. Experimental apparatus used to measure the spectral characteristics of the diode lasers.

The spectrometer is a Jarrell-Ash 0.5 m scanning spectrometer with a calculated resolution of 0.3 Å. The photomultiplier tube (PM) is an RCA 7102 with a S-1 response; it was biased at 1250 V. The output of the PM was amplified by a Keithley model 427 current amplifier, and the amplified signal was recorded on a Hewlett Packard model 680M strip chart recorder. The rise times of the amplifier and recorder did not affect the spectral resolution of 0.3 Å.

Spectral recordings of lasers THR 6 and THR 4 were made at various drive currents from threshold current to maximum rated drive current. Laser THR 7 failed before any spectral measurements could be made. The laser radiation was focused onto the slit of the spectrometer because early measurements indicated the spectral content of the laser radiation was different for different parts of the beam. A typical spectral recording is shown in Fig. 11. The plate factor of the recording is $\alpha = 1.999 \pm 0.002$ Å/cm.

The double peaks of each axial mode in Fig. 11 is caused by the two junctions in the laser with each peak being an axial mode from each

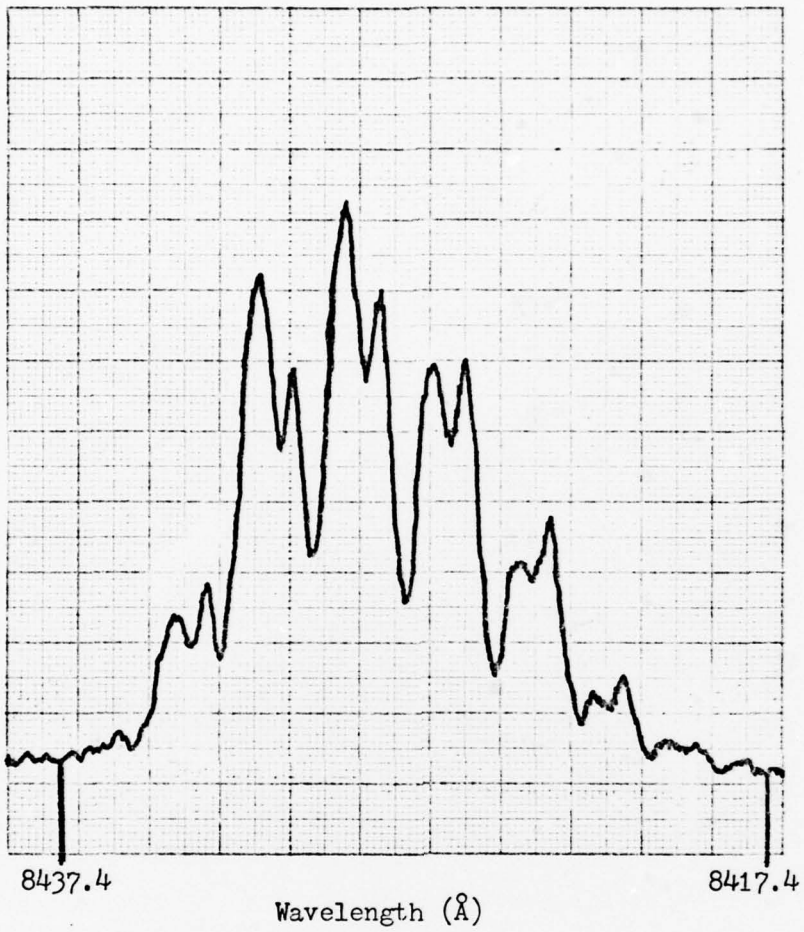

Fig. 11. Typical spectral recording of the lasers tested. Taken from laser THR 4 operated with a drive current of 2.0 A.

laser junction. This was verified by imaging the laser junctions, and recording the spectrum of each junction separately.

Table III and Table IV summarize the spectral characteristics of lasers THR 6 and THR 4 respectively. From the values contained in the Tables, the thermal impedance of the diode lasers was measured by observing the shift towards longer wavelength of $\bar{\lambda}$ with increased DC input power, $P_{in} = IxV_f$. Figure 12 shows a curve of the average

TABLE III
CW spectral characteristics of laser THR 6

Bias V_f (volts)	Drive Current I (amp)	Input Power IxV_f (watt)	Average Lasing Wavelength $\bar{\lambda}$ (Å)	Wavelength Bandwidth $\delta\lambda$ (Å)
3.00	1.2	3.6	8432.4	21.4
3.47	1.7	5.9	8437.3	39.3
3.82	2.2	8.4	8447.3	35.0
4.04	2.7	10.9	8470.1	42.7
4.22	3.2	13.5	8495.0	44.0

TABLE IV
CW spectral characteristics of laser THR 4

Bias V_f (volts)	Drive Current I (amp)	Input Power IxV_f (watt)	Average Lasing Wavelength $\bar{\lambda}$ (Å)	Wavelength Bandwidth $\delta\lambda$ (Å)
2.60	1.0	2.6	8408.1	9.9
2.83	1.2	3.4	8412.7	7.5
3.07	1.5	4.6	8415.7	18.6
3.45	2.0	6.9	8426.8	13.6
3.80	2.5	9.5	8437.2	15.7
4.05	3.0	12.2	8452.3	18.4

lasing wavelength, $\bar{\lambda}$, versus the DC input power for lasers THR 6 and THR 4. The average lasing wavelength shifts towards longer wavelengths with increased junction operating temperature because of a reduction in the bandgap energy for GaAs with increased temperature. This wavelength shift is approximately linear over the range from 77°K to 300°K, and has a value of β = 2.4 Å/°K (Ref 2: 42). Using this value, the thermal impedance of each diode is given by (Ref 2: 44),

$$R_t = \frac{\Delta\lambda}{\Delta P_{in} x \beta} \qquad (7)$$

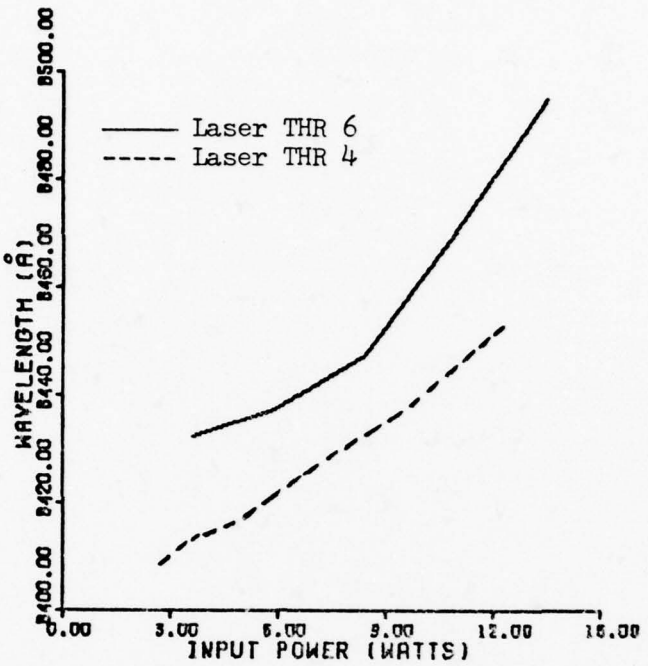

Fig. 12. Plot of wavelength shift versus input power for lasers THR 6 and THR 4.

where $\Delta\lambda/\Delta P_{in}$ is the slope of the curves in Fig. 12. For laser THR 6, this corresponds to a thermal impedance of R_t = 3.8 °K/w, and for laser THR 4, R_t = 2.0 °K/w. These values will be discussed later.

Spatial and Temporal Characteristics

The spatial and temporal characteristics of laser THR 6 were not measured because it gradually degraded during the course of the spectral measurements until its maximum output power was approximately one-half of its original value. This degradation in optical output power was accompanied by an increase in forward bias across the diode. Before replacing laser THR 6, its junctions were imaged with a 2.54 cm focal length lens (diameter 2.5 cm).

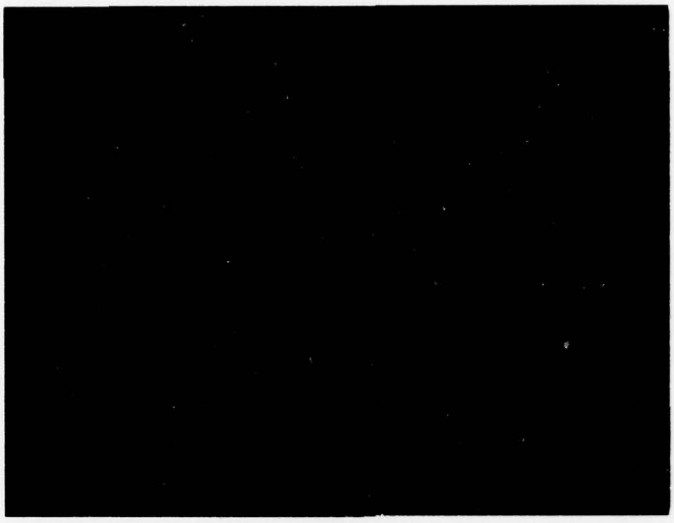

Fig. 13. Photograph of the imaged junctions of laser THR 6 at a drive current of 1.2 A. The measured magnification is 37x.

The image of the junctions was projected onto a phosphor screen located approximately two meters from the lens, and photographs of the image were made at various drive currents. Figure 13 shows the two junctions of laser THR 6 (oriented as if one were looking into the dewar) at a drive current of 1.2 A. As can be seen from Fig. 13, the upper junction is just beginning to lase. Figure 14 shows laser THR 6 at a drive current of 1.55 A. In Fig. 14, the upper junction is now fully lasing and the lower junction has just reached threshold. This corresponds to a difference in threshold current for the two junctions of approximately 0.35 A.

Fig. 14. Photograph of the imaged junctions of laser THR 6 at a drive current of 1.55 A. The measured magnification is 37x.

The curvature of the radiation pattern in Fig. 14 is caused by a lens abberation. Figure 15 shows laser THR 6 at a drive current of 3.0 A. From Fig. 15, one can see the lower junction never fully lases and has a dark region in its center.

Laser THR 6 was replaced with laser THR 7 which failed catastrophically after 5.5 hours of operation because of an experimental error. During its short life, the beam divergence in only one direction was measured. The divergence measurement of this laser was in good agreement with that of laser THR 4. Laser THR 7 was

Fig. 15. Photograph of the imaged junctions of laser THR 6 at a drive current of 3.0 A. The measured magnification is 37x.

then replaced with laser THR 4. It should be noted that prior to installing lasers THR 7 or THR 4 on the cold finger of the dewar, both the cold finger and the laser heat sink were polished with a fine emory cloth then cleaned in acetone. This provided for a good thermal contact. This procedure was not followed when laser THR 6 was installed.

After laser THR 4 was installed in the dewar, photographs of its junctions revealed a 0.2 A difference in threshold current between the two junctions with the upper junction reaching threshold first. It was also observed that only three-fourths of the lower junction exhibited lasing.

Divergence measurements of laser THR 4 were made along the x and y axes, as defined in Fig. 5, with an EG&G SGD 100A detector apertured with a 1.3 mm diameter pinhole. The detector was biased at 95 V, and its output was connected to a Tektronix 7514 oscilloscope through a 7A-22 differential amplifier. This plug-in unit was used because of its good sensitivity (10 μV). The detector was mounted on a Data Optics film plate holder which allowed two degrees of movement for the detector along the x and y axis. A scale was built into the film plate holder which could be read to an accuracy of 1.0 mm. The experimental apparatus used in the divergence measurements is shown in Fig. 16. For the

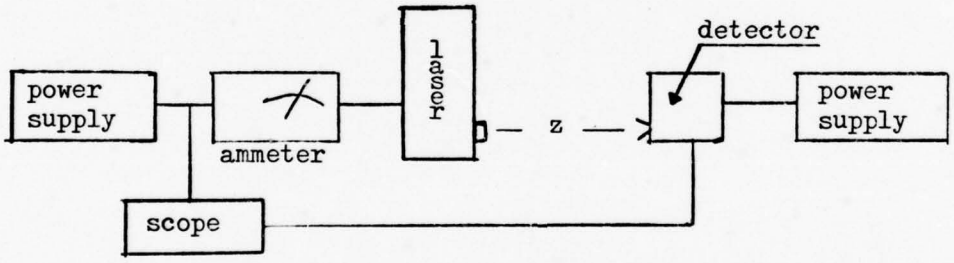

Fig. 16. Experimental apparatus used to measure the beam divergence of laser THR 4. For x divergence, z = 25.7 cm. For y divergence, z = 16.2 cm.

divergence measurements, the detector was moved along the respective axis in increments of 1.0 mm. Typical intensity profiles of laser THR 4 are shown in Fig. 17 and Fig. 18. The slight skewness in the intensity profiles in Figs. 17 and 18 are caused by a misalignment of the normal between the laser and the detector.

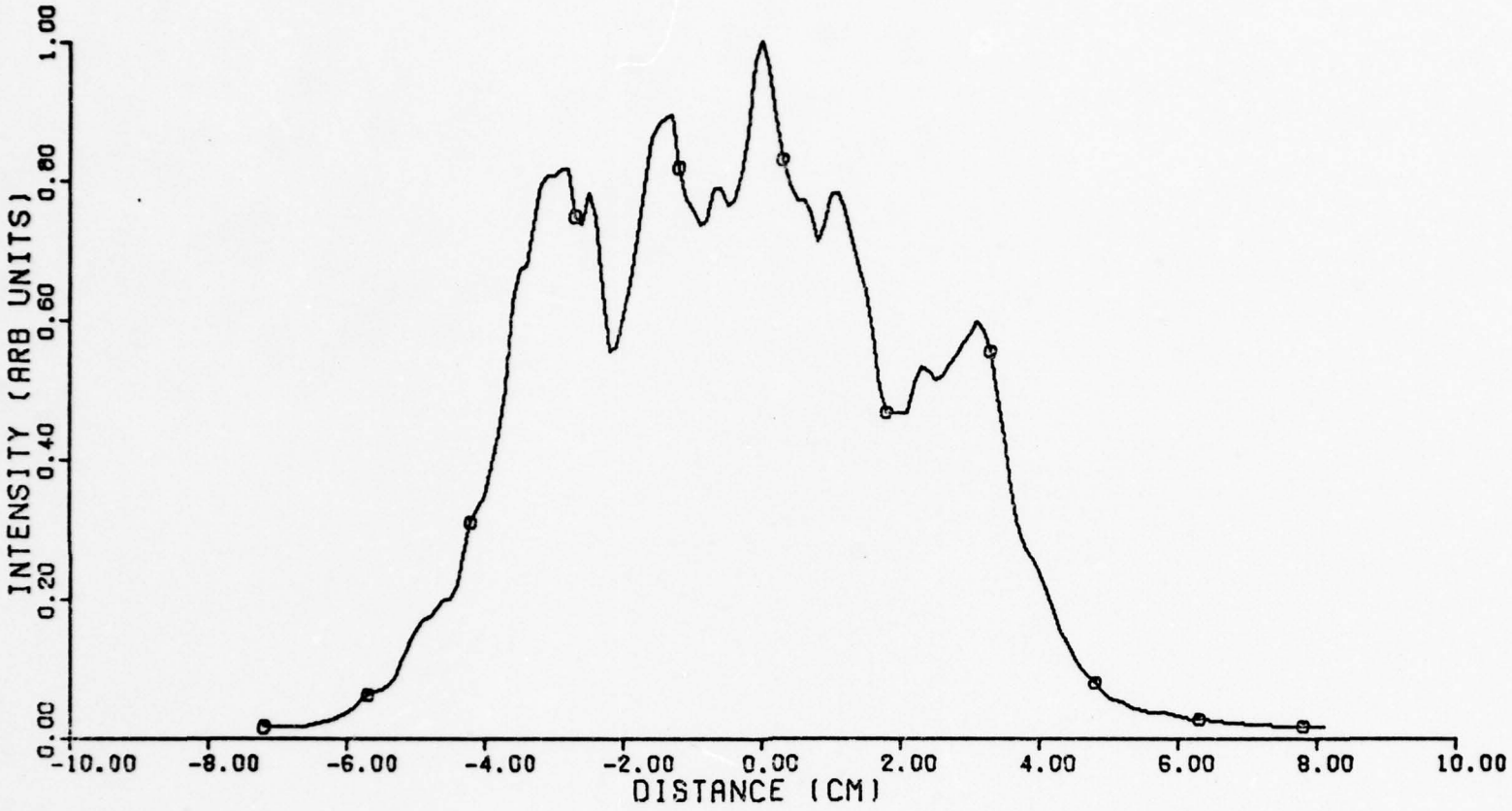

Fig. 17. Intensity profile of laser THR 4 along the x axis. The laser was operated with a drive current of 2.0 A (output power is 0.241 w). The full-angle beam divergence is 20°.

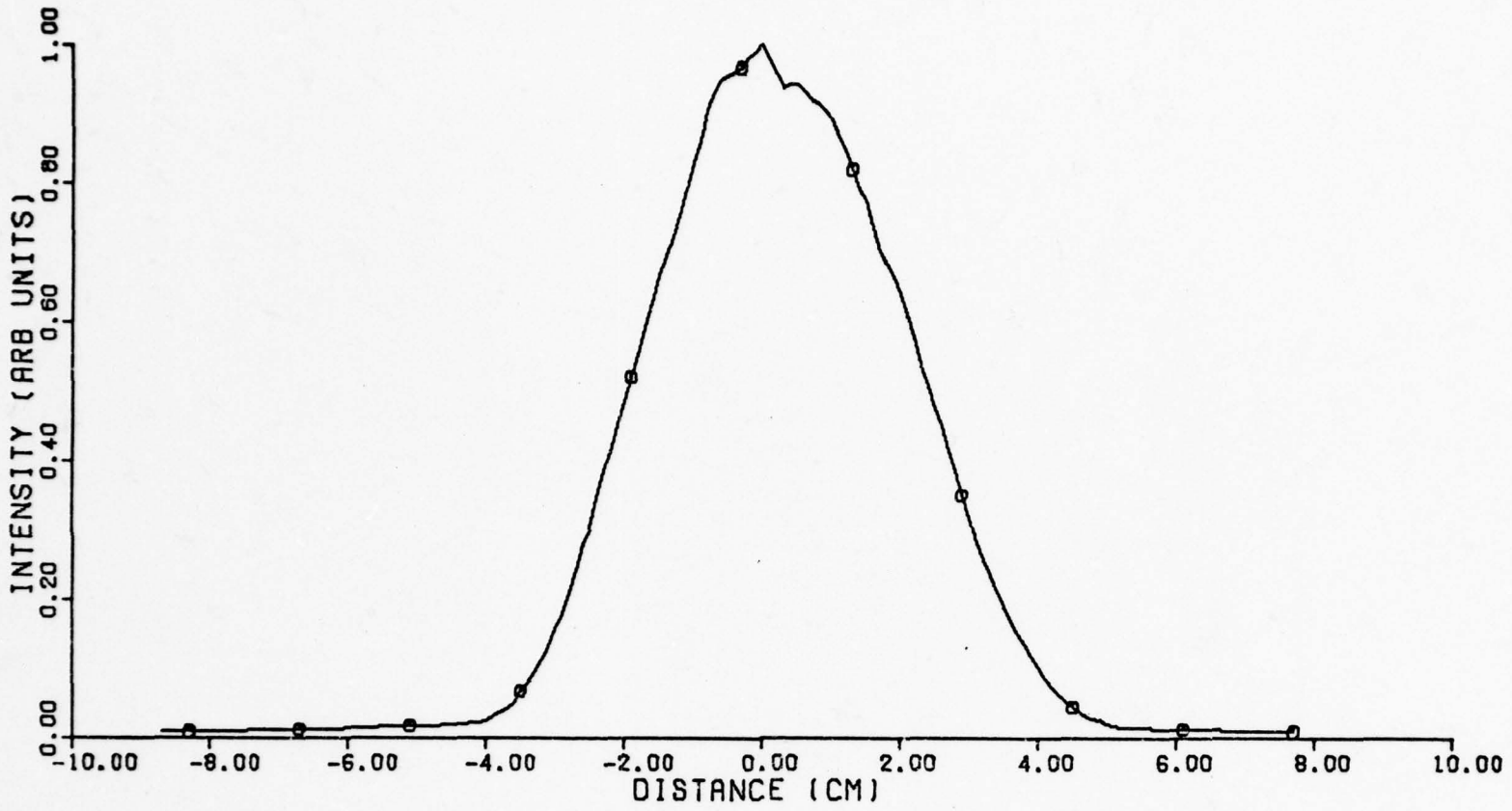

Fig. 18. Intensity profile of laser THR 4 along the y axis. The laser was operated with a drive current of 2.0 A (output power is 0.241 w). The full-angle beam divergence is 23°.

The full-angle beam divergence measurements for laser THR 4 (operated at various drive currents) are summarized in Table V.

TABLE V
Full-angle beam divergence of laser THR 4 at various DC drive currents

Drive Current I (amps)	Input Power P_{in} (watts)	Output power P_o (watts)	Full-Angle Beam Div x axis	Full-Angle Beam Div y axis
1.0	2.6	0.027	15°	24°
1.5	4.5	0.108	17°	24°
2.0	6.8	0.241	20°	23°
2.5	9.3	0.365	24°	24°

The polarization of laser THR 4 was checked with the use of a Glan-Thompson polarizer. Although the polarizer had some leakage, it was still apparent that the laser was predominantly TE polarized (the electric field vector is parallel to the junction plane). The degree of polarization (Ref 7: 44) was measured to be at least 0.65. More careful measurement with a better polarizer should yield a degree of polarization much higher than that stated in this report.

No temporal variations in the laser beam were observed for any drive current. The experimental set-up used to measure temporal variations is shown in Fig. 19. A 38 mm focal length lens was used to partially collimate the laser beam. The beam then traversed an optical path length of 4.77 m to an EG&G SGD 100A detector (rise time 5 ns) biased at 95 V. The detector had a 2.5 mm diameter aperture, and was positioned in a sensitive part of the beam so that the slightest vibration caused a deflection on the oscilloscope.

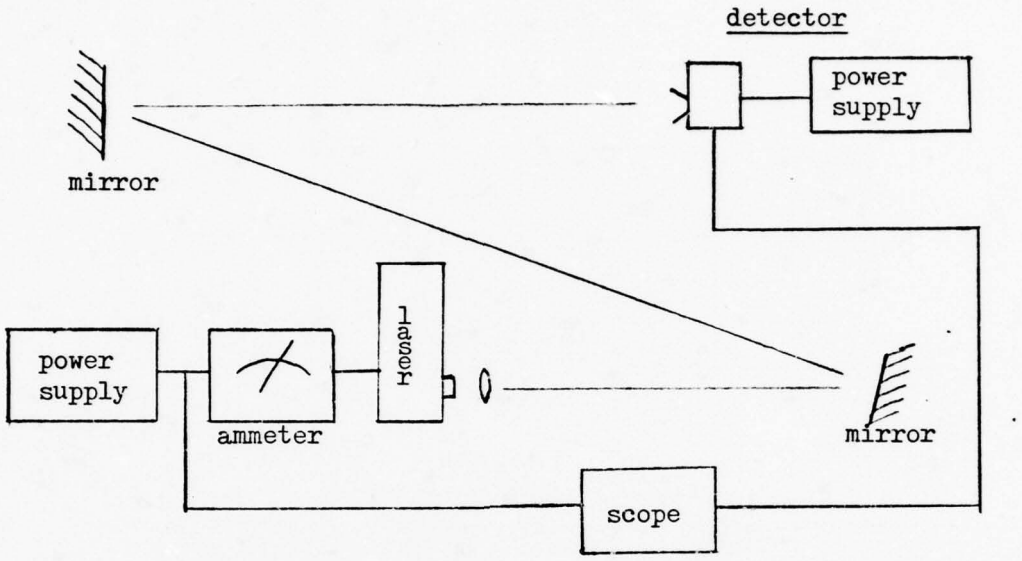

Fig. 19. Experimental set-up used to determine the temporal characteristics of the laser beam.

It was calculated that a one milliradian shift in the beam at the laser would correspond to a 0.5 mm shift of the beam position at the detector. Since no variations in the output of the detector were observed, the beam was not temporally varying in intensity; and, if the divergence was temporally varying or the beam was temporally steering, it was much less than one milliradian.

Conclusions and Recommendations

Since lasers THR 1 through THR 10 were all grown in the same melt by LPE, one would expect their output characteristics to be similar. The fact that their output characteristics are not similar indicates that thermal gradients and/or impurities were present in

the ovens during the growth phase of the GaAs lasers. Further refinement in the growth process of LPE is needed to produce GaAs lasers with consistent output characteristics.

During the spectral measurements of these devices, it became apparent that each junction acts as a separate laser, and there is no mutual interference between their respective beams. This can be explained by the difference in threshold current for each junction. It was also observed that different parts of the beam contained different spectral content. The reason for this is evident from the images obtained of the junctions while the lasers were operating. Each junction does not lase uniformly, but in filaments or separate axial modes. Across the magnified image of a junction, the axial modes appear as bright spots. This was verified when an attempt was made to image the junctions and then aperture the image to allow the radiation from only one junction to be analysed spectroscopically. Depending upon where the aperture was placed in the junction image, spectral recordings showed one or two modes present, but the multimode nature of the radiation was absent. It was then decided to focus the radiation onto the slit of the spectrometer to obtain the complete spectrum of the lasers.

The thermal impedance of laser THR 4 was significantly lower than that of laser THR 6 because of the care taken in mounting laser THR 4 onto the cold finger of the dewar. The thermal impedance

could be reduced even further if thermal grease were used between the dewar cold finger and the laser heat sink. This was not attempted because of possible outgassing of commercially available thermal grease under high vacuum.

The maximum rated drive current for each laser was specified by the manufacturer, but as can be seen in Fig. 7, the output power of laser THR 6 deviates from linearity at drive currents above 2.3 A. This roll-off in output power indicates excessive heating in the diode laser. Since a drive current of 2.3 A corresponds to an input power of approximately 9 w, the effect of this heating can also be seen in Fig. 12 where the slope of the wavelength-shift curve for laser THR 6 suddenly increases at an input power of 9 w. This could contribute to the high thermal impedance of that laser.

It is recommended that the method of rating the maximum drive current for the lasers be standardized more carefully by using the output power characteristics of the lasers.

The gradual degradation of laser THR 6 was accompanied by an increase of forward bias across the diode. This points out a problem that is peculiar to dual junction lasers made in this manner. Consider the equivalent circuit for a dual junction laser shown in Fig. 20. For DC currents, we can ignore the reactance of the junction capacitance and consider only the junction resistance. If we assume initially that the resistance of each junction is the same, then the total current through each junction will also be equal. The maximum rated drive current for this laser was $I_t = 3.5$ A or $I_1 = I_2 = 1.75$ A. Initially, the total impedance of

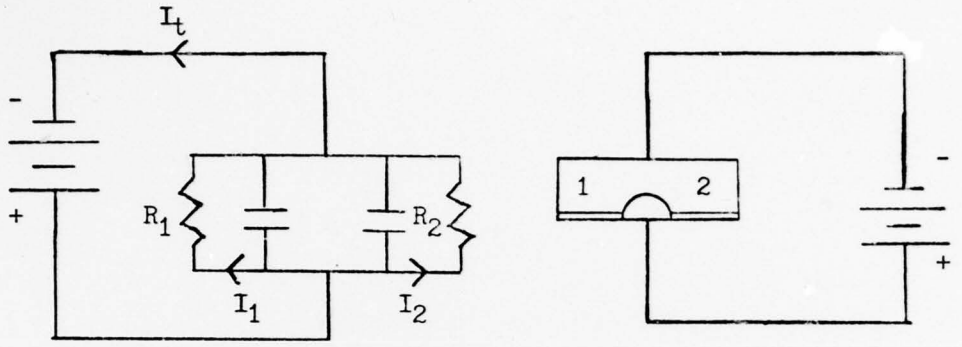

Fig. 20. Equivalent circuit for a dual junction diode laser.

the laser was

$$R_t = \left(1/R_1 + 1/R_2\right)^{-1} = 1.33 \text{ ohm} \tag{8}$$

for a forward bias of 4.00 V at 3.0 A. Therefore, at I_t = 3.0 A we have $R_1 = R_2$ = 2.66 ohm, and $I_1 = I_2$ = 1.5 A. Assuming junction two remained good and junction one degraded, we can associate all increase in forward bias with resistance changes in junction one. After approximately 15 hours of operation, the forward bias of laser THR 6 increased to 4.38 V at a drive current of 3.0 A while the output power decreased 50 per cent. Now,

$$R_t = 4.38/3.0 = 1.46 \text{ ohm} \tag{9}$$

but, since junction two remained good, R_2 = 2.66 ohm as before. Therefore,

$$R_1 = \left(1/R_t - 1/R_2\right)^{-1} = 3.24 \text{ ohm} \tag{10}$$

and

$$I_1 = 4.38/3.24 = 1.35 \text{ A} \tag{11}$$

with

$$I_2 = 4.38/2.66 = 1.65 \text{ A} \tag{12}$$

This implies that for a given drive current, a degraded junction will cause the good junction to draw more current than it would if both junctions functioned normally. Therefore, at $I_t = I_{max}$ the maximum current rating of the good junction will be exceeded causing it to degrade, and eventual failure of the laser.

This problem could be eliminated if each junction was electrically isolated from the other. Then the current through each junction could be controlled individually, and failure of one junction would not necessitate the failure of the other junction.

The increase of bulk resistance in the degraded junction of laser THR 6 is caused by a decreased electron mobility. A possible cause of this could be a dislocation through the junction region which would also explain the dark area in the center of the degraded junction seen in Fig. 15.

The divergence of laser THR 4 was essentially constant in the y direction while its divergence in the x direction increased with an increase in drive current. This is caused by an increase in the number of axial modes present across the laser junction as the drive current is increased.

The fact that laser THR 4 was predominantly TE polarized is not surprising because optical loss at a cleaved, uncoated GaAs mirror is greater for TM than for TE modes (Ref 9: 489).

Laser Characterization (RF Current-Modulated at 25 MHz)

RF Driver

The RF driver used during this experiment was a modified version of a similar driver built by Perkin-Elmer Corp (Ref 3). The RF driver as designed by Perkin-Elmer Corp could not be used because it required a lead length of one inch to the laser, and the configuration of the laser in the dewar necessitated a lead length of approximately three inches. The modification was accomplished by AFIT personnel (Ref 10), and it consisted of re-designing the tank circuit of the RF driver to compensate for the higher inductance caused by the longer lead length. A circuit schematic of the driver appears in Fig. 21.

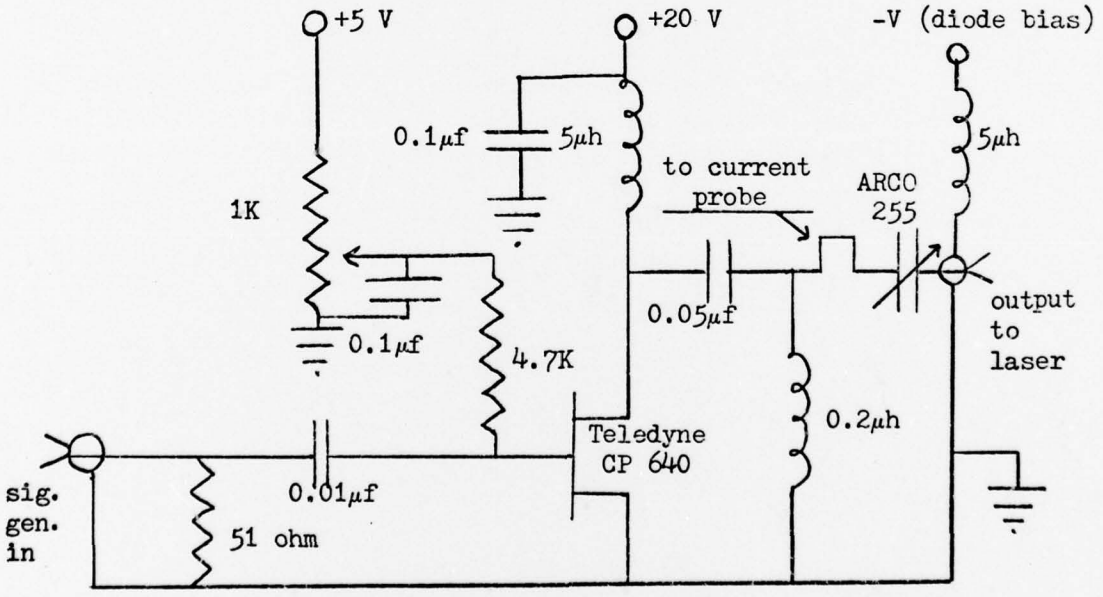

Fig. 21. Schematic diagram of the RF current modulator (Ref 10).

The maximum modulation depth (see Appendix C) of the current supplied to the laser was limited to 1.25 A by the power rating of the transistor. Two power supplies are required to power the current modulator, and require a minimum rating of 5 V at 100 ma and 20 V at 0.5 A respectively. The RF signal input to the current modulator requires a signal generator with a minimum output of 10 V peak-to-peak. The laser bias is supplied by a separate power supply (described earlier in the report) through the RF current modulator.

The modulated current supplied to the laser was monitored on the oscilloscope with the use of a Tektronix P-6042 current probe.

RF Experimental Results

Although RF current modulation of lasers THR 4, THR 10, and THR 3 was achieved, the limited life of the lasers tested precluded the obtaining of conclusive results.

The lasers exhibited stable operation under DC drive conditions, but at 25 MHz RF current modulation, the maximum life of the lasers tested was 1.5 hours for laser THR 4 which failed at a DC bias of 2.5 A and a modulation depth of 1.2 A. Laser THR 10 failed after 10 sec at a DC bias of 1.5 A and a modulation depth of 0.5 A, and laser THR 3 failed after 30 min at a DC bias of 1.4 A and a modulation depth of 0.65 A.

Prior to its failure, the output of laser THR 4 was observed to be sinusoidally modulated at 25 MHz, and the beam divergence in the y direction was measured at a DC bias of 1.5 A and 2.0 A with the current modulated to a depth of 0.3 A and 0.8 A respectively.

The full angle beam divergence of laser THR 4 under 25 MHz current modulation was the same as that shown in Table V for DC drive currents of 1.5 A and 2.0 A.

After the lasers failed, photographs were made of their front facets to determine if any physical changes occurred in the GaAs material. The photograph of laser THR 4 showed a completely destroyed diode with just fragments of the GaAs material left; however, photographs of lasers THR 10 and THR 3 are of some interest, and are shown in Fig. 22 and Fig. 23 respectively (orientation of the front facet is shown in Fig. 2).

Fig. 22. Photograph of laser THR 10 after it failed during the 25 MHz RF current modulation experiment.

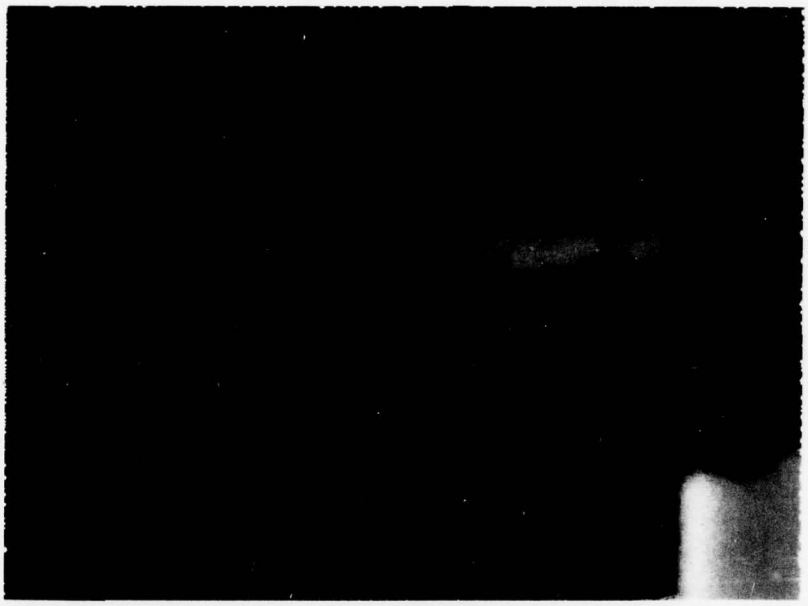

Fig. 23. Photograph of laser THR 3 after it failed during the 25 MHz RF current modulation experiment.

In Fig. 22, it appears that fractures have occurred in the GaAs material on the left junction while part of the right junction has either sheared off or disintigrated. Since laser THR 10 no longer drew any current after it failed, it is assumed that the fractures were throughout the length of the material.

Comparing Fig. 22 to that of laser THR 10 shown in Fig. A3 of Appendix A, one sees the absence of a large pitted area on the left junction and the presence of more dark spots on that junction after it was RF current-modulated.

In Fig. 23, it is clear that both junctions have fractured near the heat sink of the laser. Comparing Fig. 23 to that of laser THR 3 shown in Fig. A4 of Appendix A, one sees rather dramatic changes in the GaAs material. The left junction is practically void of the pit marks and dark spots present on it before it was RF current-modulated, and a closer inspection of Fig. 23 shows striations across the left junction of the material running from left to right.

Conclusions and Recommendations

Twenty-five megahertz RF current modulation of the diode lasers has been achieved, but their limited life under this drive condition warrants further investigation. A possible cause for their failure will be treated later in this report.

Assuming laser operation can be sustained while it is RF current-modulated at 25 MHz, experiments should be constructed to measure average output power and peak power, to determine whether the beam is temporally diverging and/or temporally steering, and to measure the phase angle of the input signal versus the optical output signal before these lasers are used as illuminators in an operational device.

In their report (Ref 3), Perkin-Elmer Corp has noted the average output power of the laser increases over its DC value when the current is RF modulated at the same DC bias. Upon analyzing their data, it was empirically determined that the increase in average output power could be related to the AC input power of the modulated current. A value for the AC input power is given

by the equation (Ref 11: 46-48)

$$P_{ac} = \frac{I_{pp}^2 R_l}{8} \tag{13}$$

where R_l is the impedance of the laser, and I_{pp} is the peak-to-peak AC current into the laser. The total input power to the laser would then be equal to them sum of the AC input power (obtained from Eq 13) and the DC input power (obtained from the DC bias). When this value is multiplied by the power efficiency of the laser, it agrees with the measured average output power to within five per cent. Although this implies the diode laser can convert AC input power to optical output power, the mechanism by which this occurs is not understood, and a theoretical study should be undertaken to verify this hypothesis.

Since GaAs is a piezoelectric material (Ref 12: 1462), it is possible that the fractured junctions in lasers THR 10 and THR 3 were due to a shear force in the lattice caused by the DC bias and 25 MHz RF current modulation. The striations observed in the front facet of laser THR 3, Fig. 23, could also have been caused by shear forces.

The GaAs lasers used during these experiments were grown such that the applied current through the material was perpendicular to the (100) crystallographic orientation (Ref 2: 12). A first order mathematical analysis (see Appendix B) shows a shear force present in the GaAs material, parallel to the junction plane, of 4.8×10^6 dynes/cm^2 per junction. The shear strength of GaAs at 300°K is 1.89×10^{10} dynes/cm^2 (Ref 13). In calculating the shear

force, the following assumptions were made:

1. The junction was an abrupt p^+n junction.

2. The bulk material one either side of the junction was GaAs.

3. No applied forward bias was present, and the electric field across the depletion region was due entirely to the contact potential of the junction.

4. All elastic constants of the GaAs material were for an operating temperature of 300°K.

5. No other forces were present in the GaAs material.

6. No RF current modulation was present.

Although the shear force calculated in the GaAs material is four orders of magnitude less than the shear strength of the material, no conclusions can be made from the mathematical analysis for the following reasons:

1. The depletion region in the diode laser is not in the GaAs layer, but in the (GaAl)As layer. The elastic constants for (GaAl)As, although thought to be similar to GaAs (Ref 13), have not (to the author's knowledge) been measured.

2. The junction region in the laser is not an abrupt p^+n junction with no forward bias, but a p^+-i-n^+ junction with a high forward bias condition. Analyses of p^+-i-n^+ junctions have been carried out under high forward bias conditions (Ref 14: 448-456), but the injection levels in these lasers may be so high that this analysis is no longer valid (Ref 14: 449).

3. The difference in thermal expansion coefficients of GaAs and (GaAl)As causes a compressive force on the GaAs epitaxial layer of 10^8-10^9 dynes/cm^2 at 300°K (Ref 1: 1534). At 77°K this force is expected to be somewhat larger, and it may change the elastic constants of the GaAs and (GaAl)As layers significantly (Ref 13); however, this force can be removed by using $(Ga_{1-x}Al_x)P_yAs_{1-y}$, with $y \approx 0.015$, instead of $(Ga_{1-x}Al_x)As$ in the respective epitaxial layers (Ref 1: 1534).

4. Although the 25 MHz RF current modulation was not near the shear mode resonant frequency of GaAs which is on the order of a gigahertz or higher (Ref 15: 259), the other factors present in this problem must also be considered in calculating the shear mode resonant frequency of the GaAs material.

Other possible causes of the junction fractures could be a shear force imposed on the laser by over-tightening the laser heat sink onto the cold finger of the dewar, or lattice defects in the lasers that would have caused the fractures from thermal cycling of the lasers.

A study should be made to determine if one or more of the possible effects discussed could have caused the lasers to fracture.

Summary

The lack of uniformity in the output characteristics of these lasers shows the need for improvement in the growth process of the ternary heterostructure material. In particular, the possibility of having temperature variations and impurities present in the growth medium should be analysed and corrected.

The method of determining the maximum rated drive current of these devices should be standardized. This, coupled with an improved procedure to mount the diodes onto the cold finger of the dewar, should significantly reduce their thermal impedances.

The use of single junction or electrically isolated dual junction diode lasers should be investigated to preclude the possibility of a degraded junction causing complete laser failure when it is operated near maximum rated drive current.

The mechanism which causes the average output power of the lasers to increase when they are RF current-modulated, although empirically related to the AC input power of the RF current signal, should be theoretically analysed to gain further insight about this phenomenon.

RF current modulation at 25 MHz caused the lasers to fail within a few hours. Photographs made of the lasers after failure occurred indicate the GaAs material sheared in the junction region. It was postulated the piezoelectric effect induced the shear in the GaAs material, and an estimate of the shear force present in the diode lasers was made using an electric field and depletion width calculated by modeling the diodes as abrupt p^+n junctions with no

forward bias. Since the estimated shear force was less than the shear strength of the GaAs material, and the lasers are in fact p^+-i-n^+ diodes under high forward bias conditions; they should be remodeled as such to obtain a more realistic value for the electric field and depletion width in the junction region. The shear force should then be re-calculated using this new model, and include the possibility of changed elastic constants due to the internal stress (caused by the lattice mismatch between the GaAs and (GaAl)As layers) of 10^8 to 10^9 dynes/cm^2 present in the GaAs material.

Bibliography

1. Panish, M. B . "Heterostructure Injection Lasers." Proceedings of the IEEE, 64, 18: 1512-1540 (October 1976).

2. Gill, R. B. and T. E. Stockton. CW GaAs Diode Lasers. AFAL-TR-76-173. Wright Patterson AFB, Ohio: Air Force Avionics Laboratory, May 1977.

3. Perkin-Elmer Corporation. Gallium Ardenide (GaAs) Diode Laser RF Experimental Results. USAF Contract No. F33615-75-C-1155. Ann Arbor, Michigan: Perkin-Elmer Corp, 1975 (Technical Report No. 13170).

4. Casey, H. C. Jr and M. B. Panish. "Composition Dependence of the $Ga_{1-x}Al_xAs$ Direct and Indirect Energy Gaps." Journal of Applied Physics, 40: 4910-4912 (November 1969).

5. Private Communication: Mennella, J. Laser Diode Laboratories, Metuchen, New Jersey (September 1977).

6. Chown, M., et al. "Direct Modulation of Double-Heterostructure Lasers at Rates Up To 1 Gbit/s." Electronics Letters, 9, 1: 34-36 (January 1973).

7. Born, M. and E. Wolf. Principles of Optics (Fifth Edition). New York: The Pergamon Press, 1975.

8. Gray, Dwight E. American Institute of Physics Handbook (Third Edition). New York: Mc Graw Hill Inc, 1972.

9. Paoli, Thomas L. "Depolarization of the Lasing Emission from CW Double-Heterostructure Junction Lasers." IEEE Journal of Quantum Electronics, 11, 7: 489-493 (July 1975).

10. Private Communication: Gergal G. AFIT, Wright Patterson AFB, Ohio (August 1977).

11. Korneff, Theodore. Introduction to Electronics. New York: Academic Press, 1966.

12. Paoli, T. L. and J. E. Ripper. "Direct Modulation of Semiconductor Lasers." Proceedings of the IEEE, 58, 10: 1457-1465 (October 1970).

13. Private Communication: Reynolds, D. C. AFAL DHR, Wright Patterson AFB, Ohio (September 1977).

14. McKelvey, John P. Solid State and Semiconductor Physics. New York: Harper and Row, 1966.

15. Heising, Raymond A. Quartz Crystals for Electrical Circuits. New York: D. Van Nostrand Co Inc, 1946.

16. Nye, J. E. Physical Properties of Crystals. London: Oxford University Press, 1966.

17. SZE, S. M. Physics of Semiconductor Devices. New York: John Wiley and Sons Inc, 1969.

18. Willardson, R. K. and A. C. Beer. Semiconductors and Semimetals Volume II Physics of III-V Compounds. New York: Academic Press, 1966.

Appendix A

Photographs of the Diode Lasers Before They Were Used

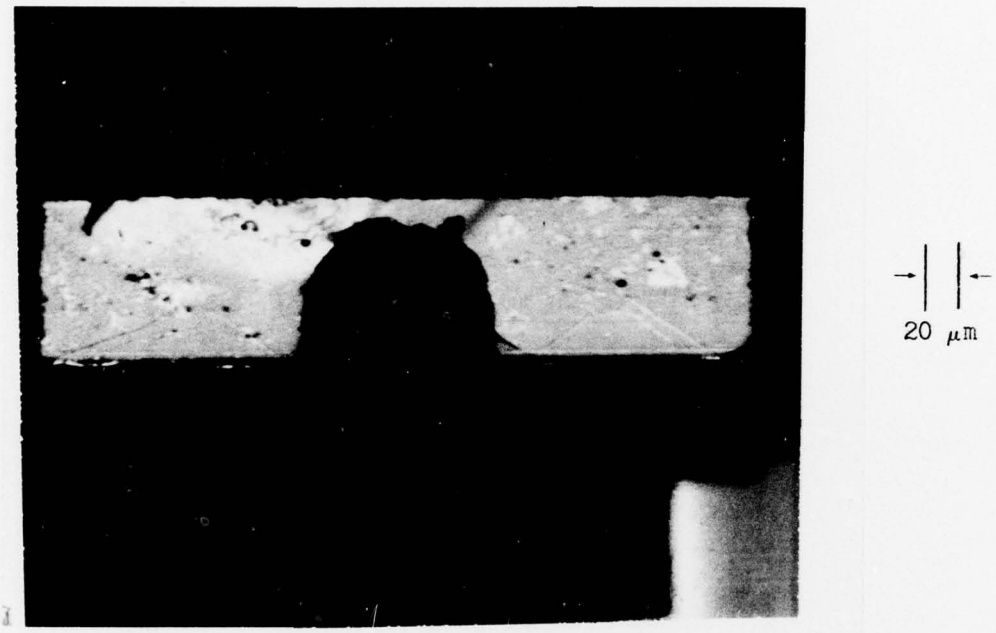

Fig. A1. Photograph of the front facet of laser THR 7 before it was installed in the dewar.

Appendix A

Fig. A2. Photograph of the front facet of laser THR 4 before it was installed in the dewar.

Appendix A

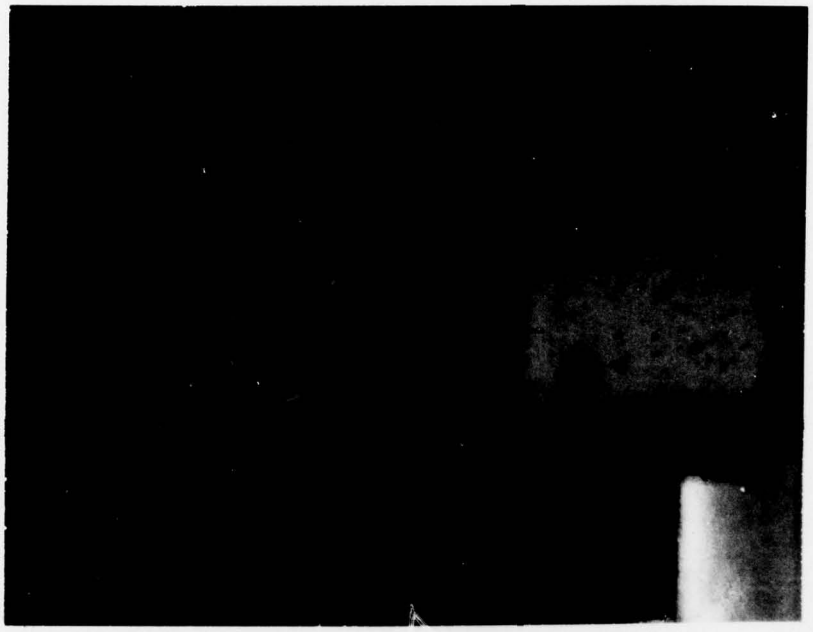

Fig. A3. Photograph of the front facet of laser THR 10 before it was installed in the dewar.

Appendix A

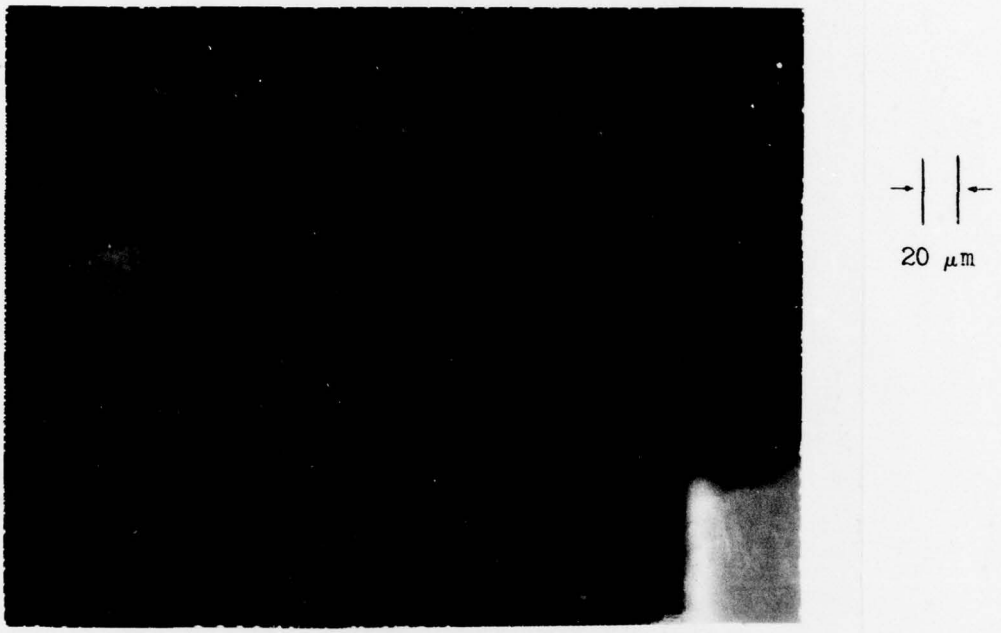

Fig. A4. Photograph of the front facet of laser THR 3 before it was installed in the dewar.

Appendix B

First Order Calculation of the Shear Force Present in the Diode Laser

GaAs is a cubic crystal with three equivalent crystallographic planes. Since the lasers used in this report were grown such that the current through the laser is perpendicular to the (100) direction (Ref 2: 12), the following analysis of the strain induced in the GaAs material will be with respect to that orientation.

The converse piezoelectric effect in the GaAs material due to the presence of an applied electric field is given by the tensor equation (Ref 16: 115),

$$\theta_{jk} = d_{ijk}E_i \tag{B1}$$

where the summation sign is understood. E_i is the applied electric field, the d_{ijk}'s are the piezoelectric moduli of GaAs, and the θ_{jk}'s are the components of the strain tensor. We choose the electric field to be perpendicular to the (100) plane across the depletion region of the diode, as it is in the actual laser. Therefore,

$$\underline{E} = \begin{pmatrix} E_1 \\ 0 \\ 0 \end{pmatrix} \tag{B2}$$

Since θ_{jk} and d_{ijk} are symmetric in j and k, we can write Eq B1 in the more convenient matrix notation as (Ref 16: 114),

$$\theta_l = d_{il}E_i \tag{B3}$$

where the d_{il} matrix for GaAs is given as (Ref 16: 124),

Appendix B

$$\underline{d} = \begin{pmatrix} 0 & 0 & 0 & d_{14} & 0 & 0 \\ 0 & 0 & 0 & 0 & d_{25} & 0 \\ 0 & 0 & 0 & 0 & 0 & d_{36} \end{pmatrix} \tag{B4}$$

Therefore, for the applied electric field, the strain tensor has only one component given by,

$$\theta_4 = d_{14}E_1 \tag{B5}$$

indicating a shear strain in the laser parallel to the junction plane (i.e. in the x_2, x_3 plane).

Having calculated the strain tensor, we can determine the shear force in the x_2, x_3 plane from the equation (Ref 16: 135)

$$\sigma_i = C_{ij}\theta_j \tag{B6}$$

where the C_{ij}'s are the stiffness constants for the GaAs crystal whose matrix takes the form (Ref 16: 140)

$$\underline{C} = \begin{pmatrix} C_{11} & C_{12} & C_{13} & 0 & 0 & 0 \\ C_{21} & C_{22} & C_{23} & 0 & 0 & 0 \\ C_{31} & C_{32} & C_{33} & 0 & 0 & 0 \\ 0 & 0 & 0 & C_{44} & 0 & 0 \\ 0 & 0 & 0 & 0 & C_{55} & 0 \\ 0 & 0 & 0 & 0 & 0 & C_{66} \end{pmatrix} \tag{B7}$$

Since the strain tensor is represented by the following matrix,

$$\underline{\theta} = \begin{pmatrix} 0 \\ 0 \\ 0 \\ \theta_4 \\ 0 \\ 0 \end{pmatrix} \tag{B8}$$

we have a shear force given by,

$$\sigma_4 = C_{44}\theta_4 = C_{44}d_{14}E_1 \text{ dynes/cm}^2 \tag{B9}$$

E_1 is given by,

$$E_1 = V_T/W \tag{B10}$$

where V_T is the total forward bias across the depletion region, and W is the width of the depletion region.

From Fig. 1, we see the pn junction is formed between layers four and five. Since the doping concentration in layer five is two orders of magnitude higher than that in layer four, we can assume the depletion region lies entirely in layer four, and model the pn junction as an abrupt p^+n one sided junction (Ref 17: 89).

In this case, the width of the depletion region is given by (Ref 17: 88-90),

$$W = \left[\frac{2\epsilon_s(V_{bi} - V)}{qN_B}\right]^{\frac{1}{2}} \tag{B11}$$

where ϵ_s is the dielectric constant of GaAs, $10.9x\epsilon_o$, V_{bi} is the contact potential, 1.25 V (Ref 17: 88), q is the electron charge, N_B is the doping concentration of layer four, 10^{16} cm^{-3}, and V is the applied forward bias.

The width of the depletion region for no applied forward bias is W = 0.4 μm. This corresponds to an electric field of $E_1 = 1.25/0.4x10^{-6} = 3.1x10^6$ V/m.

Appendix B

The resulting shear force on the GaAs material is given by Eq B9 where $C_{44} = 5.94 \times 10^{11}$ dynes/cm^2 (Ref 18: 112), and $d_{14} = 2.6 \times 10^{-12}$ m/V (Ref 8: 9-114).

Therefore, for the contact potential, the shear force is $\sigma = 4.8 \times 10^{6}$ dynes/cm^2.

Appendix C

Definition of Modulation Depth

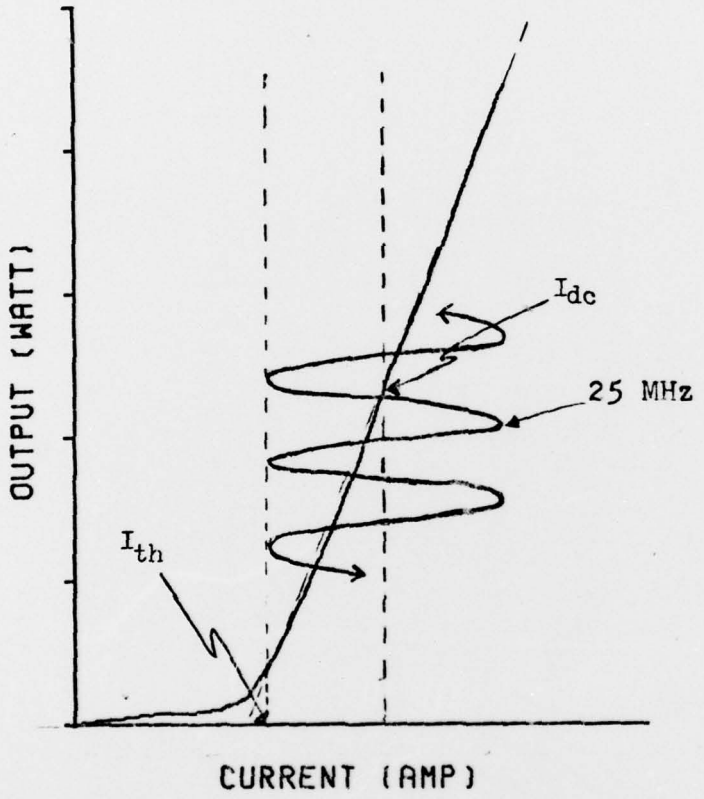

Fig. C1. Graph illustrating the definition of modulation depth.

The modulation depth is defined as one-half of the peak-to-peak value of the modulated current signal when the current signal is modulated to I_{th}. Therefore, the modulation depth, I_m, is given by

$$I_m = I_{dc} - I_{th} \qquad (C1)$$

Vita

Captain Daniel J. Murawinski was born on 18 September 1949 in Jersey City, New Jersey, the son of John S. Murawinski and Ann M. Murawinski. After graduating from Saint Peter's Preparatory School in Jersey City, he attended Stevens Institute of Technology. He graduated in 1971 with the degree of Bachelor of Science in Physics. He was commissioned that same year as a 2nd Lt, and attended pilot training at Williams AFB, Arizona. After graduating from pilot training in 1972, Capt Murawinski flew the C-130E Hercules at Pope AFB, North Carolina, until his admission into AFIT. Capt Murawinski is married, and has two daughters.

Unclassified

SECURITY CLASSIFICATION OF THIS PAGE (When Data Entered)

REPORT DOCUMENTATION PAGE		READ INSTRUCTIONS BEFORE COMPLETING FORM
1. REPORT NUMBER GEP/PH/77-9	2. GOVT ACCESSION NO.	3. RECIPIENT'S CATALOG NUMBER
4. TITLE (and Subtitle) CHARACTERIZATION OF HIGH POWER GaAs LASERS		5. TYPE OF REPORT & PERIOD COVERED MS Thesis
		6. PERFORMING ORG. REPORT NUMBER
7. AUTHOR(s) Daniel J. Murawinski, Capt, USAF		8. CONTRACT OR GRANT NUMBER(s)
9. PERFORMING ORGANIZATION NAME AND ADDRESS Air Force Institute of Technology (AFIT-EN) Wright-Patterson AFB, Ohio 45433		10. PROGRAM ELEMENT, PROJECT, TASK AREA & WORK UNIT NUMBERS C2204F 2001 01 71
11. CONTROLLING OFFICE NAME AND ADDRESS		12. REPORT DATE Dec 1977
		13. NUMBER OF PAGES 64
14. MONITORING AGENCY NAME & ADDRESS(if different from Controlling Office) Air Force Avionics Laboratory Air Force Systems Command, USAF Wright-Patterson AFB, Ohio 45433		15. SECURITY CLASS. (of this report) Unclassified
		15a. DECLASSIFICATION/DOWNGRADING SCHEDULE

16. DISTRIBUTION STATEMENT (of this Report)

Approved for public release; distribution unlimited.

17. DISTRIBUTION STATEMENT (of the abstract entered in Block 20, if different from Report)

18. SUPPLEMENTARY NOTES

Approved for public release; IAW AFR 190-17

Jerral F. Guess, Capt, USAF
Director of Information

19. KEY WORDS (Continue on reverse side if necessary and identify by block number)

GaAs
Laser
Semiconductor
III-V Compound
Piezoelectric

20. ABSTRACT (Continue on reverse side if necessary and identify by block number)

High power, cryogenically operated, dual cavity, ternary heterostructure, GaAs lasers are characterized under CW and 25 MHz RF current modulation conditions. The CW characteristics that are measured include: power, spectral, spatial, and temporal characteristics. It is calculated that degradation of one cavity will cause complete laser failure when the laser is operated near maximum rated drive current due to the dual cavity structure of these devices.

RF current modulation at 25 MHz causes the lasers to fail within a few

DD FORM 1 JAN 73 1473 EDITION OF 1 NOV 65 IS OBSOLETE

Unclassified

SECURITY CLASSIFICATION OF THIS PAGE (When Data Entered)

hours, although the same lasers exhibited stable operation under CW drive conditions. It is postulated that the piezoelectric effect in the GaAs material causes the rapid degradation, but further refinements in the calculation of the shear force present in the GaAs material is needed before definite conclusions can be made. The increase in the average output power of the GaAs lasers, operated with RF current modulation, is empirically related to the AC input power of the signal, but the mechanism by which this can occur is not understood.